6th European Conference on Computational Mechanics (ECCM 6)
7th European Conference on Computational Fluid Dynamics (ECFD 7)
11 – 15 June 2018, Glasgow, UK

DEVELOPMENT OF MULTI-SCALE MODELLING FOR CEMENTITIOUS MATERIALS DAMAGED BY EXPANSION CRACK TO EVALUATE SIZE DEPENDENCY OF SULFATE ATTACK

TAITO MIURA[1], HIKARU NAKAMURA[2] AND YOSHIHITO YAMAMOTO[3]

[1] Department of Civil Engineering, Nagoya University
Furo-cho, Chikusa-ku, Nagoya, Japan
t.miura@civil.nagoya-u.ac.jp and http://concrete-lab.civil.nagoya-u.ac.jp/homepage/j/en/index.html

[2] Department of Civil Engineering, Nagoya University
Furo-cho, Chikusa-ku, Nagoya, Japan
hikaru@nagoya-u.jp

[3] Department of Civil Engineering, Nagoya University
Furo-cho, Chikusa-ku, Nagoya, Japan
y.yamamoto@civil.nagoya-u.ac.jp

Key words: 3D-Rigid Body Spring Model, Truss Network Model, Sulfate Attack, Diffusion-Reaction Model, Expansion Cracking Behavior, Size Dependency.

Abstract. In this study, the analytical investigation using the analytical system coupled with hydration model, diffusion-reaction model and crack propagation model were conducted in order to validate the size effect of sulfate attack. This analytical system can reconstruct hydration process, transformation of liquid-solid phase and manifestation and propagation of expansion cracking behavior due to sulfate attack. Using this analysis, the transformation of solid phase and expansion crack of mortar specimens, which cross-section area were 10x10, 20x20 and 40x40 mm, were evaluated in order to clarify the size effect of sulfate attack precisely. As a result, this analytical system can evaluate the difference of expansion behavior due to cross-section area and visualize stress distribution and expansion cracking behavior in cross-section area. Furthermore, it can be said that the size effect of expansion cracking behavior due to sulfate attack could be interpreted by the internal constraint due to remaining compressive stress.

1 INTRODUCTION

It is well-known that cementitious materials constructed in certain environments including sulfate ions chemically react with sulfate ions which either weakens the cement hardened body or causes an expansion cracks, or both. These phenomena are generally called by external sulfate attack and this deterioration mainly comes from sulfate salt such as gypsum and ettringite ([1], [2]). The mechanisms of sulfate attack have been understood and two hypotheses were suggested to explain how to generate expansion pressure. The swelling theory proposed by Mehta [3] said that expansion pressure can generate as ettringite absorbs water molecule which increases the volume of ettringite. On the other hand, the crystallization pressure theory

proposed by Wellman et al. [4] and applied to sulfate attack by Flatt and Scherer [5], explains the expansibility due to ettringite as process in which after that ettringite becomes supersaturated in pore solution and crystallization starts, ettringite crystal grows in a pore and expansion pressure generates since it gets in contact with pore wall. Many researchers have contributed in order to judge which hypothesis is adequate and consistent with the experimental results under several conditions. To date, there is no consensus on which theory is more applicable. This further suggests that sulfate attack is a complicated phenomenon that is linked to diffusion, reaction (dissolution and precipitation), and mechanics.

In previous study, the numerical analytical system, which can reconstruct hydration process, transformation of solid-liquid phase and manifestation and propagation of expansion cracking behavior, is proposed (Miura *et al*. [6]). This analytical system is composed of a hydration model using *Computational Cement-Based Material model* (CCBM) (Maruyama *et al*. [7]) that can predict the change in solid phase, porosity, and mechanical behaviors due to hydration; a diffusion-reaction model that can predict transportation of sulfate ion and transformation of solid-liquid phase due to sulfate attack; and RBSM which can evaluate expansion cracking behavior. In this paper, we investigate how expansion behavior is influenced by size effect due to sulfate attack.

2 ANALYTICAL MODEL

The analytical flow of modeling sulfate attack is shown in **Figure 1**. This analysis is composed of CCBM for hydration process, diffusion-reaction model for sulfate attack, and RBSM for manifestation and propagation behavior of expansion crack. The complete details of these modeling approaches will be shown in the succeeding sections.

2.1 Cement Hydration Model

CCBM is one of the cement hydration model proposed by Maruyama et al. [7]. This model has been constructed by physical and chemical properties that can influence to the hydration process of cementitious material under different relative humidity and temperature based on many experimental data. CCBM can predict phase assemblage, porosity, strength of cement paste and concrete in a hydration process under several conditions. In this section, the capillary porosity, pcap0, is estimated by subtracting gel porosity from total porosity. Indeed, gel porosity was defined as the difference between molecular volume of C1.7SH2.5 and C1.7SH4.0. The details of the physical properties can be found in Maruyama et al. [7].

2.2 Diffusion-Reaction Model

The authors have proposed diffusion-reaction model for sulfate attack by using finite volume method. Intrinsically, all of aluminate phase can be involved into the reaction of ettringite. These reaction rate constants, however, are not yet fully understood. In this model, sulfate attack is simply described by a reaction rate with regard to the reaction between sulfate ion and portlandite because dissolved portlandite involves both precipitation reactions of ettringite and gypsum.

The concise model for sulfate attack is shown in **Figure 1**. It is assumed that the aluminate phase consumed by the reaction of ettringite is only monosulfate. Then, the precipitation reaction of ettringite which reacted with sulfate ion, portlandite and monosulfate, and the

reaction of gypsum are modeled.
Ion transfer and consumption with regards to sulfate ion in cement matrix are modeled by Equation (1).

$$\frac{\partial\left(p_{cem}\cdot C_{liquid}\right)}{\partial t}=\frac{\partial}{\partial x}\left(D\frac{\partial\left(p_{cem}\cdot C_{liquid}\right)}{\partial x}\right)+\frac{\partial C_{solid}}{\partial t} \tag{1}$$

where, C_{liquid}, is the concentration of sulfate ion in liquid phase (mol/l); C_{solid}, is the concentration of sulfate ion in solid phase (mol/l); D, is a diffusion coefficient of sulfate ion (mm^2/sec); and p_{cem}, is the porosity in cement paste (cm^3/cm^3).
Based on Garboczi and Bentz [8] study, the influence of the change in pore structure can be introduced using Equation (2).

$$\frac{D}{D_0}=0.001+0.07\cdot {p_{cap}}^2+1.8\cdot H\left(p_{cap}-0.18\right)^2 \tag{2}$$

where, D_0, is the diffusion coefficient of sulfate ion in dilute solution (mm^2/sec); and $H(x)$, is the Heaviside function (if x>0, $H(x)$=1, if x≤0, $H(x)$=0).
The reaction with sulfate ion and portlandite is defined using Equation (3).

$$\frac{\partial C_{solid}}{\partial t}=-\sum\left(K_{CH}\cdot CH_{cem}\cdot C_{liquid}\right) \tag{3}$$

where, K_{CH}, is the coefficient value of reaction rate of portlandite ($cm^3/g/sec$); and CH_{cem}, is the amount of portlandite in cement paste (g/cm^3).

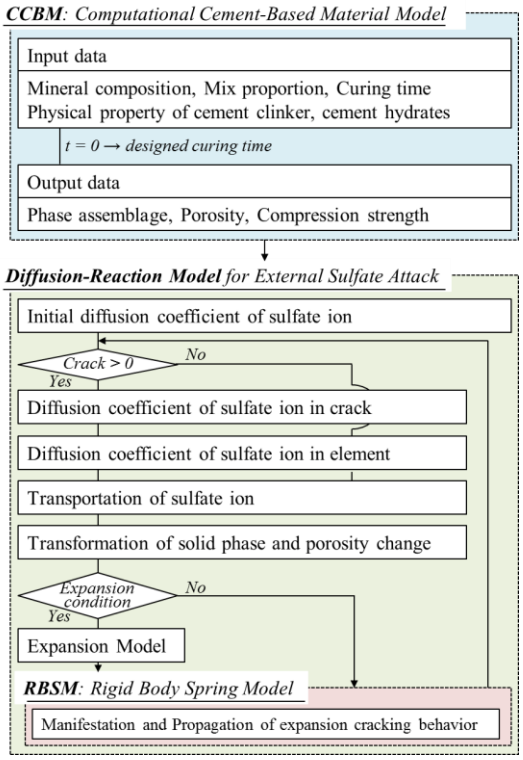

Figure 1: Analytical flow

2.3 Expansion Pressure Model

The expansion model is represented such that the expansion strain can generate the corresponding amount of ettringite. In addition, it is known that after the supersaturation of ettringite, ettringite crystal precipitates in the pore solution and expansion pressure is generated whenever the crystal gets into contact with pore wall as mentioned above. Then, the introduced time lag in the expansion model which suggests that expansion pressure will begin to generate when the ratio of temporal porosity to certain porosity at averaged volume becomes lower than threshold porosity ratio named as p_{TH} in reference to Tixier et al. [9, 10] and Ikumi et al. [11]. The expansion strain is estimated by the amount of effective ettringite which is able to contribute to the expansion pressure derived by subtracting "the temporal amount of ettringite" with "the amount of ettringite in cement paste at previous time step" (ETT- ETT_{pre}.)

$$\varepsilon_{ex} = \alpha \cdot \left(ETT - ETT_{pre} \right) \tag{4}$$

where, ε_{ex}, is the expansive strain, α, is the conversion factor of expansive strain (cm^3/g); ETT, the temporal amount of ettringite in cement paste (g/cm^3); ETT_{pre}, the amount of ettringite in cement paste at previous time step (g/cm^3).

2.4 Calculation of Porosity

Porosity should be changed corresponding to the change in solid phase such as portlandite, monosulfate, ettrignite, and gypsum. The calculation equation of porosity in cement paste and capillary porosity are provided in Equations (5) and (6). In addition, after cracking, in calculating the total porosity to compare it with the experimental results, the volume of crack has to be considered. Using RBSM, the volume of crack can be calculated from the change in crack width and the area of boundary surface of each element as shown in Equation (7). Then, the total porosity can be calculated using Equation (8).

$$p_{cem} = p_{cem0} + \left(V_{CH} + V_{AFm} - V_{ETT} - V_{GYP} \right) \tag{5}$$

$$p_{cap} = p_{cap0} + \left(V_{CH} + V_{AFm} - V_{ETT} - V_{GYP} \right) \tag{6}$$

$$V_{cra} = \frac{\sum w_i \cdot A_i}{V} \tag{7}$$

$$p_{total} = p_{cem} \cdot P_{vol} + V_{cra} \tag{8}$$

where, p_{cem0} is the initial porosity in cement paste (cm^3/cm^3); V_{CH} and V_{AFm} are the solid volume reduction in cement paste due to consumption of portlandite and monosulfate (cm^3/cm^3), respectively; V_{ETT} and V_{GYP} are the solid volume increment due to precipitation of ettringite and gypsum (cm^3/cm^3), respectively; V_{cra} is the volume ratio of crack to total volume of specimen (cm^3/cm^3); w_i is the crack width of ith boundary surface (mm); A_i is the area of ith boundary surface (mm); V is the volume of each element(cm^3); p_{total} is the total porosity in mortar (cm^3/cm^3) ; and P_{vol} is the coefficient factor of the amount of cement paste.

2.5 Crack Propagation Analysis

In this study, expansion cracking behavior is evaluated using three-dimensional RBSM

which is one of the discrete analyses proposed by Kawai [12]. **Figure 2** shows the voronoi particle definition of one RBSM element. The rigid body element is discretized using random voronoi mesh. One normal spring and two shear springs are set at integration points defined on element's boundary surface in which numerical constitutive law are introduced allowing the evaluation of crack propagation and crack width with a high degree of accuracy. **Figure 3** shows the material models of mortar. Tensile and compression models, and shear models are set into normal springs and shear springs, respectively, where, f_t is the tensile strength; E is the elastic modulus; G_f is the tensile fracture energy; τ is the shear strength; G is the shear stiffness; and f_c' is the compressive strength. The adopted compression model of normal spring is based on Yamamoto et al. [13]. Prior to the analytical investigation, compression test of cylindrical specimen is modeled, and compression and tensile strength are evaluated using RBSM in order to determine the mechanical properties at mesoscale. If we attain the mechanical properties of experiment, these coefficient values of mechanical properties are then decided in a way that is consistent with the compression and tensile test of experiment and analysis. Otherwise, we have to define macroscopic mechanical properties from f_c' calculated by CCBM and the coefficient values set based on Yamamoto et al. [13].

The expansion strain, introduced at every normal spring as initial strain, is shown in Equation (9). This expansion strain should be imposed uniformly to the normal springs set at every integration points on the boundary surfaces and is used to calculate by the amount of ettringite at the pyramid which consists of the center of element and boundary surface area as will be described later.

$$\varepsilon_T = \varepsilon_N + \varepsilon_{ex} \tag{9}$$

where, ε_T total strain, and ε_N is the strain of normal spring, respectively.

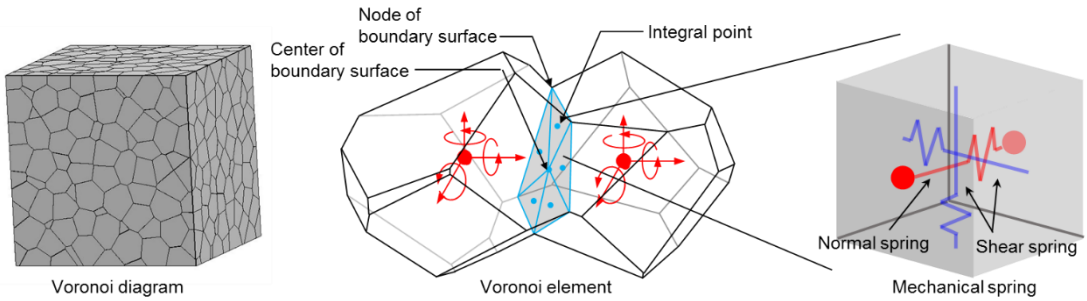

Figure 2: Overview of RBSM

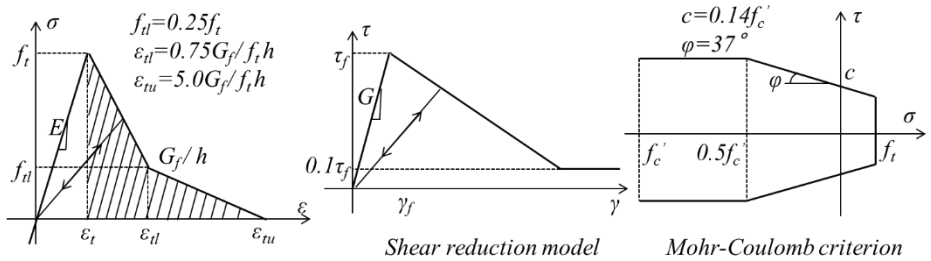

(a) tensile response (b) shear response

Figure 3: Stress-strain relationships of mechanical springs

2.6 Truss Network Model

Diffusion-reaction model for sulfate attack and RBSM can be coupled by Truss Network Model as proposed by Nakamura et al. [14]. In this model, one-dimensional pipe elements, which cannot be influenced mechanically, are set between the center of element and the center of boundary surface (E_{p1}), and between the center of boundary surface and the center of line constructing boundary surface (E_{p2}). This is done in order to describe ion diffusion between the element and a crack, and between crack to an adjacent crack as shown in **Figure 4**. E_{p1} represents ion transfer in element and E_{p2} represents ion transfer in crack. Before cracking, sulfate ion can transfer into only E_{p1}. After cracking, sulfate ion can transfer not only in E_{p1} but also in E_{p2} corresponding to a crack width. In addition, the temporal solid phase in each pyramid is calculated from temporal sulfate ion content in E_{p1}.

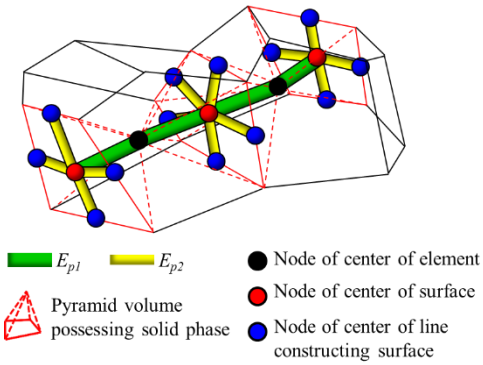

Figure 4: The arrangement of Truss Network Model

3 ANALYTICAL OBJECTIVE AND CONDITION

In this paper, the expansion behavior due to sulfate attack is verified by comparing the experimental results referred from Cheng et al. [15]. The description of the objective experimental and analytical condition is explained as below.

In the objective experiment, the mix proportion of mortars, which were made from mix proportion in reference to EN196-1 [16], are shown in **Table 1**. The mortars were immersed in sodium sulfate solution and the mineral composition of cement (CEM I 52.5) is also shown in **Table 1**. The concentrations of sulfate ion were 3 g/L and curing time was 90 days. The experimental parameter was cross-section area of specimen, which size were 10x10, 20x20 and 40x40 mm.

In our proposed analysis, analytical model was focused on center part of cross section area of mortar and was constructed by voronoi element as shown in **Figure 5**. The cross-section area was set to 10x10, 20x20 and 40x40 mm and the average element size was 1.0 mm as shown in **Figure 5(b)**. Mix proportion and mineral composition shown in **Table 1** were introduced to CCBM as input data and the change in phase assemblage, porosity, and f_c' were predicted. In addition, the input data for diffusion-reaction model was a solid phase, and porosity calculated by CCBM and diffusion coefficient of sulfate ion is in dilute solution. D_0 was set to $2.0\text{x}10^{-9}$ m^2/s in reference to Lorthenbach et al. [18]. In this study, since the information about the expansion cracking behavior and the mechanical characteristics such as f_c' is not available, the

analytical parameters for expansion cracking behavior; K_{CH}, p_{TH} and α were set to 0.01, 0.95 and 10.0 as expansion cracking behavior at cross-section area was close to the experiment by El-Hachem et al. [19] and f_c' was estimated by CCBM. The macroscopic and mesoscopic mechanical properties are shown in **Table 2**. f_t is defined as one-tenth of f_c'. E and G_f were estimated using JSCE standard [17]. The coefficient values were used based on Yamamoto et al. [13].

Table 1: Mineral composition and mix proportion of objective experiment

CEM I 42.5	**Mineral Composition (g/100g)**	**EN196-1 [16]**	**Mix proportion (kg/m^3)**
C_3S	65.8	W	266
C_2S	16.5	C	483
C_3A	6.6	S	1450
C_4AF	7.2	W/C (%)	0.55
$CaSO_3$	2.2	S/C (%)	3.0

Table 2: Constitutive law of RBSM

	Macroscopic constitutive law	**Mesoscopic constitutive law**	**Coefficient factor (meso/macro)**	**Note**
f_c' (MPa)	48.15	72.23	1.5	CCBM
f_t (MPa)	4.82	3.86	0.8	$0.1f_c'$
E (GPa)	32.6	45.64	1.4	JSCE [17]
G_f (N/m)	0.04584	0.02292	0.5	JSCE [17]
c (MPa)	—	6.74	$0.14\,f_c'$	Yamamoto [13]

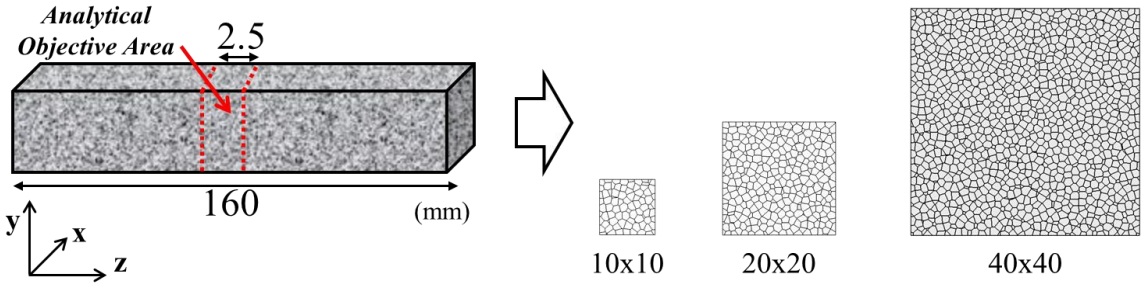

(a) specimen size (b) analytical model

Figure 5: Analytical model

4 ANALYTICAL RESULTS

The first page has to include the Editorial Heading, as shown in the first page of these instructions. Successive pages will include the name of the authors.

4.1 Phase Assemblage, Porosity and Compressive Strength before Sulfate Attack

The change in phase assemblage, total porosity, and capillary porosity in mortar and f_c' due to hydration process calculated by CCBM are shown in **Figures 6 and 7**.

As shown in **Figure 6**, in the initial stage, ettringite produced in conjunction with the consumption of C_3A and gypsum. After gypsum was completely consumed, ettringite decreased by the reaction of monosulfate and it completely transformed to monosulfate during few days. In addition, the amount of portlandite and C-S-H increased along with time in association with the consumption of C_3S and C_2S. As shown in **Figure 7(a)**, it can be confirmed that the total porosity and capillary porosity decreased with time after the curing time was about 0.15 days. After 28 days curing, total porosity and capillary porosity were found to be 0.192 and 0.090 cm^3/cm^3, respectively. As shown in **Figure 7(b)**, f_c' increases with time until a curing time of about 0.15 days and the increment of f_c' gradually decreased as well as the porosity. The f_c' after 90 days is found to be 48.15 MPa.

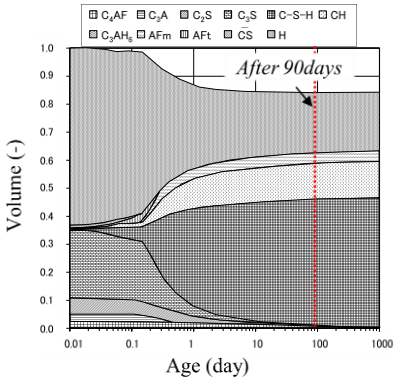

Figure 6: Phase assemblage of hydration process

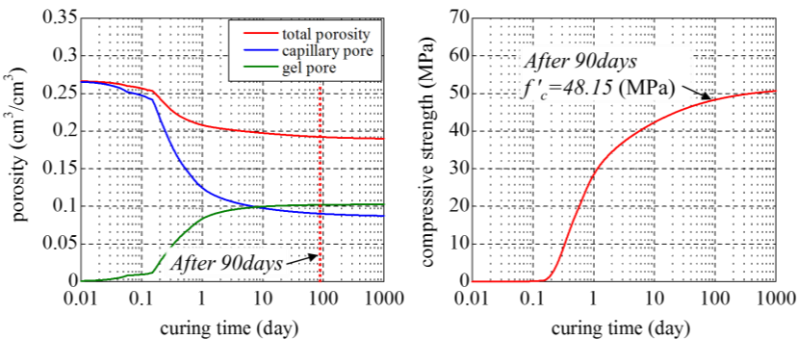

(a) porosity (b) compressive strength

Figure 7: The change in porosity and compressive strength

4.2 The Change in Solid-Liquid phase due to Sulfate Attack

The distribution of gypsum, ettringite and monosulfate in solid phase and sulfate ion in liquid phase at the depth from the surface to 5mm of the center of cross-section area after 0, 50 and 100 days immersion are shown in **Figure 8**.

According to transformation of solid phase (**Figures 8(a) ~ (c)**), it is found that the distributions of gypsum, ettringite and monosulfate are very close to each other and these tendencies are in independent to the difference of cross-section area. In particular, in case of 10x10 mm, ettringite and monosulfate are also precipitated at deeper area in comparison to 20x20 and 40x40 mm cases. As shown in **Figure 8(d)**, it is also confirmed that sulfate ion in case of 10x10 mm can penetrate deeper area than the other cases. These differences are attributed to that sulfate ion can also penetrate from opposite side surface because of small

cross-section area and transformation of solid phase can be easy to occur in comparison to the other cases. In addition, according to sulfate ion distribution, the results of 50 days immersion are close to 100 days immersion one. This tendency could be interpreted by that penetrated sulfate ion is consumed by transformation of solid phase, especially gypsum precipitation and its penetration could be retarded.

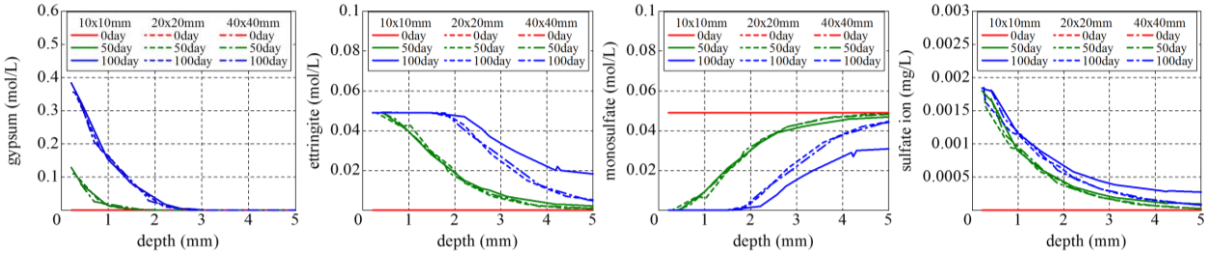

(a) gypsum (b) ettringite (c) monosulfate (d) sulfate ion

Figure 8: The change of transformation of solid phase and sulfate ion

4.3 Expansion Cracking Behavior

The change in expansion behavior is shown in **Figure 9**. Besides, expansion is calculated by the deformation in X-axis direction divided by initial width. According to this figure, it is clearly found that the expansion is bigger as cross-section area is smaller. These tendencies are similar to experimental results [15]. However, the expansion rate is bigger than objective experimental results, the final expansion rate in case of 10x10, 20x20 and 40x40 mm cases are 4.5, 8.5 and 7.0 times of experiment one, respectively. In fact, the definition of expansion of analysis is different from experiment. The experimental expansion is calculated by the longitudinal deformation but, in analysis, it is calculated by circumferential deformation. In the future, we will try to figure out the expansion behavior three-dimensional expansion behavior in order to clarify the relationship between expansion behavior and expansion cracking behavior.

Next, the reason why the size effect of expansion behavior due to sulfate attack will be discussed by using stress distribution, deformation and cracking behavior as shown in **Figure 10**. In case of 10x10 mm case, the tensile stresses are appeared at surface area and compressive stresses are also appeared at inner area of cross-section area after 30 days. As immersion time increases, tensile stresses generate at inner area and compressive stresses generate dispersedly and both stresses gradually decrease until 120 days. In case of 20x20 and 40x40 mm cases, the tensile stresses mainly appear at the surface area and gradually become advanced inward as well as 10x10 mm case. On the other hands, the compressive stresses after 120 days are still existing at cross-section area. According to cracking distribution, expansion crack after 120 days reaches to center part of cross-section area in case of 10x10 mm case. However, in case of 20x20 and 40x40mm cases, expansion crack remained at near the surface area. These differences could influence to the expansion behavior as shown in **Figure 9**. That is to say, when cross-section area is smaller, the compressive stresses at inner area diminish earlier and expansion crack is easy to occur because internal constraint become smaller at cross-section

area. On the other hands, when cross-section area is bigger, the compressive stresses at inner area still remain and expansion crack cannot propagate to inner area comparatively because internal constraint still maintains at cross-section area. Thereby, it can be said that the size effect of expansion cracking behavior due to sulfate attack could be interpreted by the internal constraint due to remaining compressive stress.

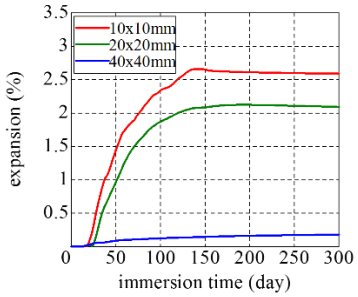

Figure 9: The change in expansion behavior in X-axis direction

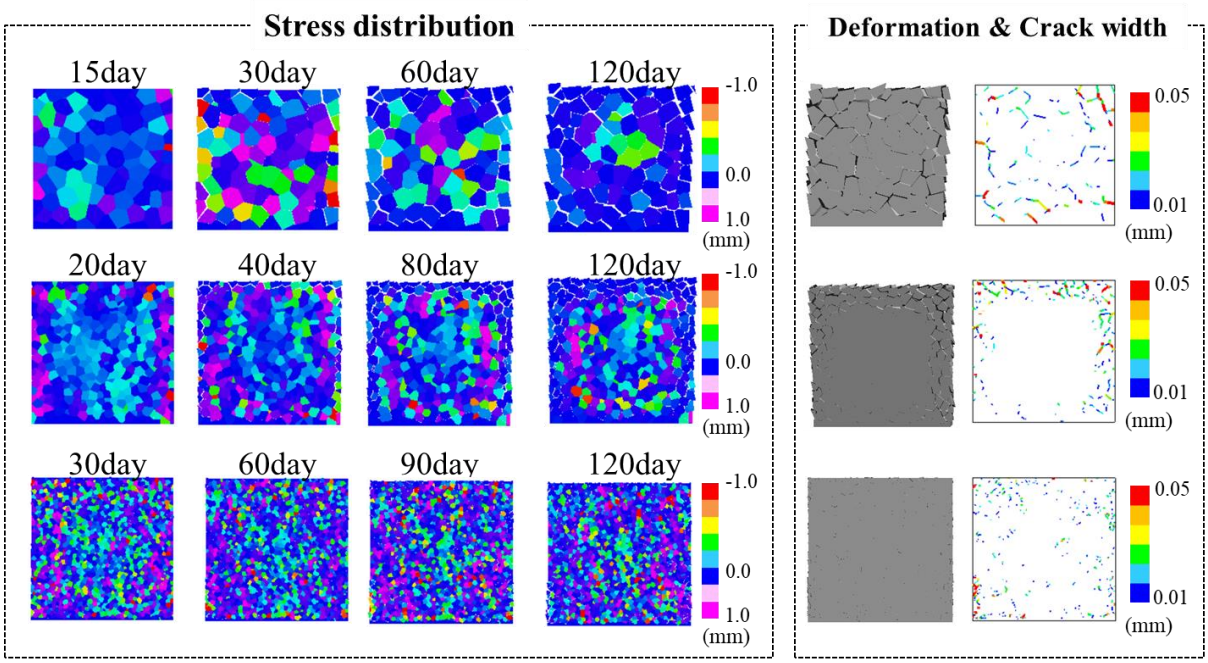

Figure 10: The distribution of stress distribution, deformation and crack width

5 CONCLUSION

In this paper, the size effect of expansion cracking behavior due to sulfate attack was evaluated by proposed analytical system. As a result, it was found that the change in expansion rate of smaller cross-section area became bigger although the area of transformation of solid was independent of the difference of cross-section area. Furthermore, according to stress distribution and expansion crack distribution, the compressive stresses at inner area diminished earlier and expansion crack was easy to occur when cross-section area was smaller. On the other hands, when cross-section area was bigger, the compressive stresses at inner area still remained

and expansion crack cannot propagate to inner area comparatively because internal constraint was still maintained at cross-section area. Therefore, the size effect of expansion cracking behavior due to sulfate attack could be interpreted by the internal constraint due to remaining compressive stress.

6 ACKNOWLEDGMENTS

Parts of this paper were funded by Grant-in Aid for Young scientists (B). The authors would like to thank the financial support.

REFERENCES

[1] Taylor H. F. W. Cement chemistry 2nd edition, *Thomas Telford*, (1997).
[2] Skalny J., Marchand J. and Odler I. Sulfate attack on concrete, *Modern Concrete Technology 10*, (2002).
[3] Mehta P.K. Mechanism of expansion associated with ettringite formation, *Cement and Concrete Research*, Vol.3, pp.1-6, (1973).
[4] Wellman H. W., Wilson A. T. Salt weathering a neglected geological erosive agent in coastal and arid environments, *Nature*, Vol. 205, pp. 1097-1098, (1965).
[5] Flatt R. J., Scherer G. W. Thermodynamics of crystallization stresses in DEF, *Cement and Concrete Research*, Vol.38, pp.325-336, (2008).
[6] Miura T., Maruyama I., Nakamura H., Yamamoto Y., Feedback system of ion transfer through cracks during deterioration of mortar due to sulfate attack evaluated by RBSM-TRUSS NETWORK MODEL, *Journal of Advanced Concrete Technology*, Vol. 15, pp.610-626, (2017).
[7] Maruyama I., Igarashi G. Numerical approach towards aging management of concrete structures: Material strength evaluation in a massive concrete structure under one-sided heating, *Journal of Advanced Concrete Technology*, Vol.13, pp.500-527, (2015).
[8] Garboczi E. Z., Bentz D. P. Computer simulation of the diffusivity of cement-based materials, *Journal of Materials Science*, Vol.27, pp.2083-2092, (1992).
[9] Tixier R., Mobasher B., ASCE, Modeling of Damage in Cement-Based Materials Subjected to External Sulfate Attack. I: Formulation, *J. Mater. Civ. Eng.*, Vol.15 (4), pp.305-313, (2003).
[10] Tixier R., Mobasher B., ASCE Modeling of Damage in Cement-Based Materials Subjected to External Sulfate Attack. II: Comparison with Experiments, *J. Mater. Civ. Eng.*, Vol.15 (4), pp.314-322, (2003).
[11] Ikumi T., Cavalaro S.H.P., Segura I., Aguado A. Alternative methodology to consider damage and expansions in external sulfate attack modeling, *Cement and Concrete Research*, Vol.63, pp.105-116, (2014).
[12] Kawai T. New discrete models and their application to seismic response analysis of structure, *Nuclear Engineering and Design*, Vol.48, pp.207-229, (1978).
[13] Yamamoto Y., Nakamura H., Miura T. Numerical Analyses of Seismic Response of a Reinforced Concrete Building Using Discrete Model with Random Geometry, *WORKSHOP SMART2013*, (2014).
[14] Nakamura H., Srisoros W., Yashiro R. Kunieda M. Time-Dependent Structural Analysis

Considering Mass Transfer to Evaluate Deterioration Process of RC Structures, *Journal of Advanced Concrete Technology*, Vol.4, No.1, pp.147-158, (2006).
[15] Cheng Y. Wei S., Scrivener K. Mechanism of expansion of mortars immersed in sodium sulfate solutions, *Cement and Concrete Research*, Vol.43, pp.105-111, (2013).
[16] European Standard, EN196-1, method of testing cement Part-1: Determination of strength, (1994).
[17] JSCE Standard specifications for concrete structures-Design, (2012).
[18] Lothenbach B., Bary B., Bescop P. L., Schmidt T., Leterrier N. Sulfate ingress in Portland cement, *Cement and Concrete Research*, Vol.40, pp.1211-1225, (2010).
[19] El-Hachem R., Roziere E., Grondin F., Loukili A. Multi-criteria analysis of mechanism of degradation of Portland cement based mortars exposed to external sulphate attack, *Cement and Concrete Research*, Vol. 42, pp.1327-1335, (2012).